Electron and hole centres in the x-irradiated elpasolite crystal Cs_2NaYCl_6 studied by means of electron paramagnetic resonance and electron nuclear double resonance

1997 J. Phys.: Condens. Matter 9 8737

(http://iopscience.iop.org/0953-8984/9/41/018)

J. Phys.: Condens. Matter **9** (1997) 8737–8747. Printed in the UK PII: S0953-8984(97)84243-9

Electron and hole centres in the x-irradiated elpasolite crystal Cs_2NaYCl_6 studied by means of electron paramagnetic resonance and electron nuclear double resonance

Th Pawlik and J-M Spaeth

University of Paderborn, FB Physik, 33098 Paderborn, Germany

Received 13 May 1997

Abstract. We report on the first investigation of radiation-induced defects in the cubic elpasolite Cs_2NaYCl_6 produced by low-temperature x-irradiation. Upon x-irradiation at 30 K a V_K-type hole centre and an electron centre identified as Y^{2+} are formed. The Y^{2+} centre is stable up to 70 K. At this temperature it recombines with a proportion of the V_K centres. The remaining V_K centres decay at approximately 150 K. The properties of the V_K centre in Cs_2NaYCl_6 are very similar to those of the V_F centre in NaCl. The Y^{2+} centre can be described by a Jahn–Teller distorted $4d^1$ ground state. In ENDOR experiments, evidence was found for a reorientation of the $Y^{2+}Cl_6$ centre complex.

1. Introduction

Hexahalogenide elpasolites with the structural composition Cs_2NaRX_6 (where X is a halogen ion and R can be a rare-earth, actinide, yttrium or indium ion) have been the subject of numerous optical and magnetic studies.

They are attractive because of the almost unique feature that the R^{3+} ions are each located at the centre of a regular octahedron formed by the six neighbouring chlorine ions. This structure provides a natural cubic environment for the incorporation of trivalent dopants. Therefore, different trivalent rare-earth [1–6] and transition elements [7] have been incorporated. The crystal structure of Cs_2NaYCl_6 is shown in figure 1.

The isostructural hexafluoride composition Cs_2NaYF_6 doped with Ce^{3+} or Pr^{3+} was found to be an efficient x-ray storage phosphor [8]. The radiation defects responsible for the storage phosphor mechanism were studied in [9]. In the hexafluoride compound, F centres are produced by x-irradiation. These centres serve as the photostimulable electron centres in the storage phosphor mechanism. In the hexachloride, however, x-irradiation produces no F centres.

The subject of this paper is the investigation of intrinsic x-irradiation-induced defects in the hexachloride Cs_2NaYCl_6.

2. Experimental procedure

Single crystals of Cs_2NaYCl_6 were grown by the vertical Bridgman method using stoichiometric amounts of CsCl, NaCl and YCl_3. The crystals are hygroscopic and show no

0953-8984/97/418737+11$19.50

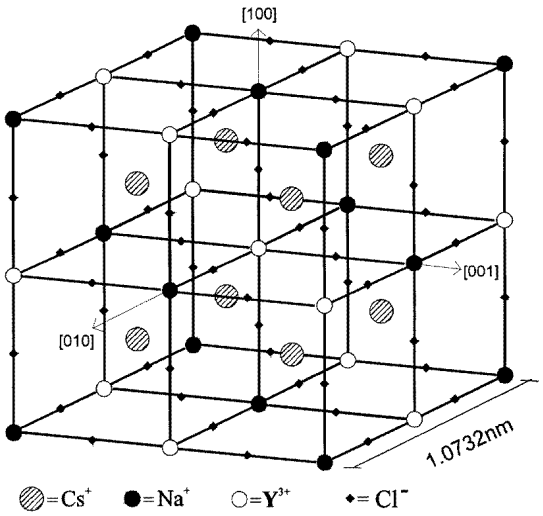

Figure 1. The crystal structure of the cubic elpasolite Cs_2NaYCl_6.

cleavage planes. Thus, they were oriented using the Laue method. Electron paramagnetic resonance (EPR) and electron nuclear double resonance (ENDOR) experiments were carried out on a custom-built spectrometer operating in the X band. The samples were x-irradiated in the EPR/ENDOR cryostat *in situ* at low temperatures using a portable Philips x-ray tube (60 kV, 15 mA). EPR and ENDOR measurements could be made after x-irradiation without subsequent warming of the crystal.

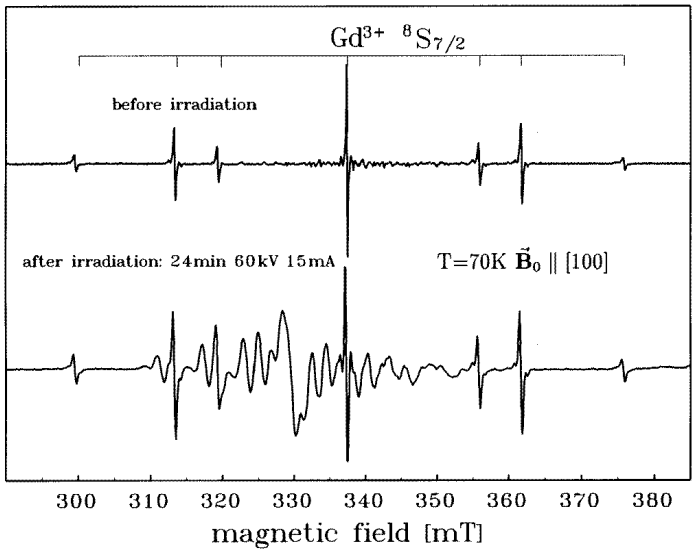

Figure 2. The X-band EPR spectrum ($\nu = 9.387$ GHz) of the V_K centre in Cs_2NaYCl_6 for $\boldsymbol{B} \parallel [100]$. Upper trace: before x-irradiation; lower trace: after x-irradiation at 77 K.

3. The V_K centre in Cs_2NaYCl_6

After x-irradiation at liquid nitrogen (LN_2) temperature a new complex EPR spectrum is observed in the $g \approx 2$ region. Figure 2 shows the EPR spectrum of Cs_2NaYCl_6 with $\boldsymbol{B}_0 \parallel [100]$ before and after irradiation at LN_2 temperature. Paramagnetic Gd^{3+} ($S = 7/2$) was present as an impurity. By measuring the angular variation of the EPR spectrum, the radiation-induced defect could be identified as a V_K centre (a Cl_2^--type hole centre where the unpaired electron is shared between two adjacent Cl^- ions) [10, 11]. The splitting in the EPR spectrum arises from the anisotropic hyperfine (hf) interaction of the unpaired spin with the two Cl nuclei. The hf interaction has a maximum when $\boldsymbol{B}$ is parallel to the Cl–Cl ($\langle 110 \rangle$) axis and it is almost zero when $\boldsymbol{B}$ is perpendicular to it. The EPR spectrum can be described by the following spin Hamiltonian [12]:

$$\boldsymbol{H} = \mu_B \boldsymbol{S}\mathbf{g}\boldsymbol{B} + \sum_{j=1}^{2} (\boldsymbol{I}_j \mathbf{A}_j \boldsymbol{S}_j - g_{n_j}\mu_n \boldsymbol{B}) \tag{1}$$

where the sum runs over the two Cl nuclei.

Since chlorine has two isotopes, ^{35}Cl and ^{37}Cl with 75% and 25% abundance, respectively, the majority of the V_K centres are of the form ^{35}Cl–^{35}Cl. These centres give a seven-line EPR spectrum with an intensity ratio of 1:2:3:4:3:2:1 for each of the six different $\langle 110 \rangle$ orientations of the V_K centre.

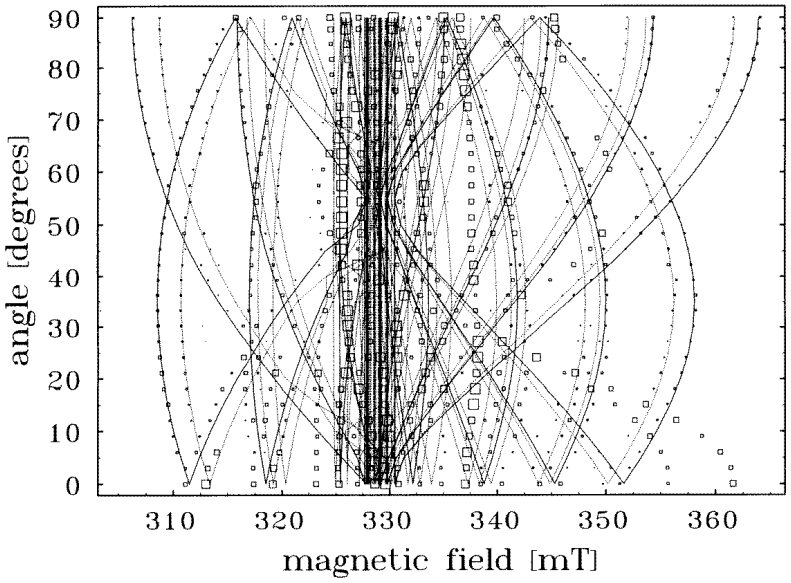

Figure 3. The EPR angular dependence of the V_K centre in Cs_2NaYCl_6. The crystal was rotated in a $(01\bar{1})$ plane. The squares indicate the experimental line positions, and the solid and dotted lines are the calculated line positions of the V_K centres with the compositions ^{35}Cl–^{35}Cl and ^{35}Cl–^{37}Cl, respectively. The interaction parameters for the calculation are those of table 1. The additional EPR lines at around 360 mT are Gd^{3+} lines.

Figure 3 shows the EPR angular dependence of V_K in Cs_2NaYCl_6 with the magnetic field rotated in a $(01\bar{1})$ plane.

Table 1. The g-tensor and hf interaction parameters of the V_K centre in Cs_2NaYCl_6 and NaCl [11]. The hf parameters are given for the ^{35}Cl isotope.

V_K centre in:	$g_\parallel$	$g_\perp$	$a_\parallel/h$ (MHz)	$a_\perp/h$ (MHz)
Cs_2NaYCl_6	2.001 ± 0.001	2.036 ± 0.001	269.6 ± 0.5	12 ± 2
NaCl	2.0010 ± 0.0001	2.0457 ± 0.0001	274	16

The g-tensor and hf parameters of the V_K centre in Cs_2NaYCl_6 are listed in table 1. They are very similar to those of the V_K centre in NaCl [11] which are listed in table 1 for comparison. This is not surprising because the interionic distance is very similar. However, other than in NaCl, in elpasolite crystals there are two possible sites for the V_K centre: the nearest neighbour of the V_K centre can either be a sodium ion or an yttrium ion. Therefore, ENDOR investigations were carried out in order to resolve the superhyperfine (shf) interactions with the neighbouring shells.

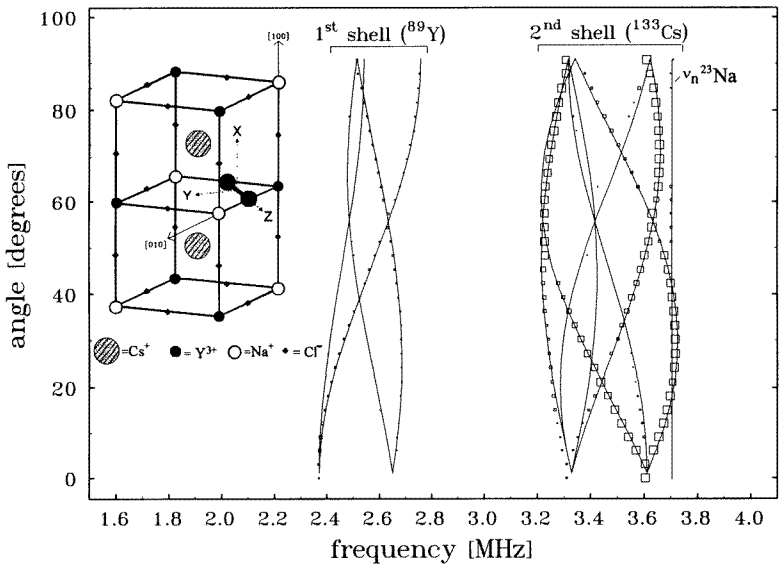

Figure 4. The angular dependence of the ^{89}Y and ^{133}Cs ENDOR lines ($m_S = -1/2$) of the first two neighbour shells of the V_K centre in Cs_2NaYCl_6. The crystal was rotated in a $(01\bar{1})$ plane.

3.1. ENDOR measurements

ENDOR measurements were carried out at 10 K on the central EPR transition at $g \approx 2$. Figure 4 shows the ENDOR angular dependence of the V_K centre (for the crystal rotated in a $(01\bar{1})$ plane) with ENDOR lines from the first shell (^{89}Y) and the second shell (^{133}Cs) of neighbours. The assignment to the different nuclei was made by varying the magnetic field and by measuring the shift in frequency of a particular ENDOR line due to the nuclear Zeeman interaction [12]. The parameters of the shf interaction with those two shells are listed in table 2.

Table 2. Superhyperfine interaction parameters of the ^{133}Cs and ^{89}Y shell of the V_K centre in Cs_2NaYCl_6. α, β and γ are the angles of the principal axes of the shf tensor with respect to the V_K-centre principal axes (see figure 4).

Shell	A_{xx}/h (MHz)	A_{yy}/h (MHz)	A_{zz}/h (MHz)	α (deg)	β (deg)	γ (deg)
Y	3.36 ± 0.01	4.14 ± 0.01	3.71 ± 0.01	0	90	90
Cs	3.77 ± 0.01	2.75 ± 0.01	2.96 ± 0.01	29 ± 2	29 ± 2	0

Apart from the Larmor frequency ν_n, no ENDOR lines due to interactions with ^{23}Na nuclei were observed. Thus, we conclude that the V_K centres produced by x-irradiation at LN_2 temperature stabilize next to an Y^{3+} ion.

By measuring the EPR excitation spectrum of a particular ENDOR line it is possible to separate the EPR spectra of different V_K-centre orientations. The measurements show that the predicted EPR spectra of V_K centres with their axes at an angle of 45 degrees with respect to the magnetic field orientation differ from the observed spectra, as there are additional splittings of the seven-line hf structure. The additional splittings can be explained by a deviation of the g- and hf tensor axes from the 45° (Cl–Cl) axis by about 4°.

This 'bent bond' is possible because of the lower local symmetry of the V_K centre in Cs_2NaYCl_6 (C_{2v}) compared to NaCl (D_{2h}). A similar bent-bond configuration is found also for the V_F centre in NaCl which is a V_K centre with a reduced C_{2v} symmetry due to an alkali vacancy in the nearest neighbourhood [13].

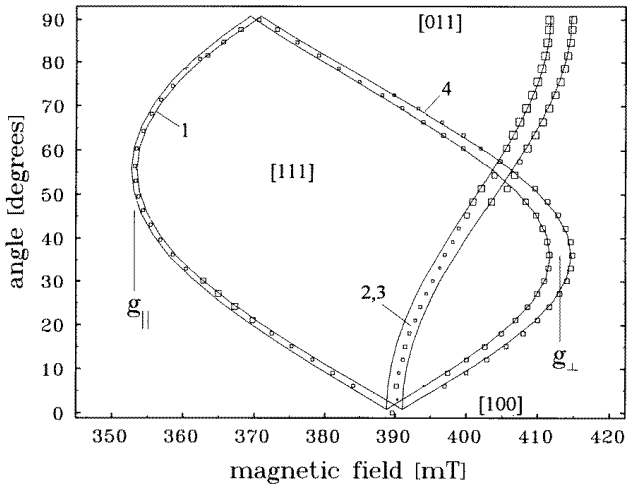

Figure 5. The EPR angular dependence of the trigonal Y^{2+} centre A. The crystal was rotated in a $(01\bar{1})$ plane.

4. Low-temperature electron centres

After irradiation at $T = 20$ K, no EPR signals due to F centres were observed. Instead there was evidence for two electron centres in the $g < 2$ region which have similar EPR spectra. The intensity ratio of these centres, called henceforth A and B, is about 10:1. Each centre

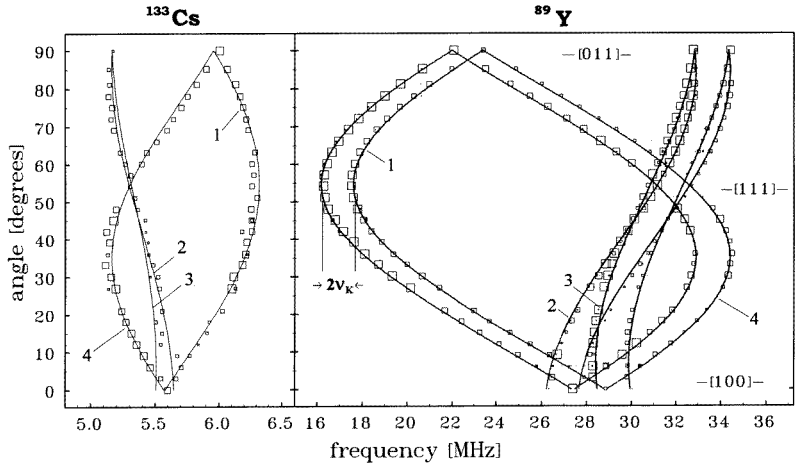

Figure 6. The angular dependence of the ^{89}Y (right) and ^{133}Cs (left) ENDOR lines of the trigonal Y^{2+} centre A. The ENDOR spectra were measured for all EPR transitions. The crystal was rotated in a $(01\bar{1})$ plane. A small misalignment leads to a splitting of lines. The solid lines represent the ENDOR angular dependence calculated using the interaction parameters given in table 3.

Table 3. The g-tensor and shf interaction parameters of the Y^{2+} centres A and B in Cs_2NaYCl_6.

Centre	$g_\parallel$	$g_\perp$	$a(^{89}Y)/h$ (MHz)	$b(^{89}Y)/h$ (MHz)	$a(^{133}Cs)/h$ (MHz)	$b(^{133}Cs)/h$ (MHz)
A	1.900 ± 0.001	1.623 ± 0.001	56.15 ± 0.05	-11.18 ± 0.05	6.58 ± 0.02	0.98 ± 0.02
B	1.927 ± 0.001	1.658 ± 0.001	56 ± 5	$(-)28 \pm 5$	—	—

exhibits an anisotropic EPR spectrum. The angular dependence of centre A is shown in figure 5. Apart from the small splitting of EPR lines at higher magnetic fields, the angular dependence can be described by an $S = \frac{1}{2}$ system with an anisotropic g-tensor with trigonal $\langle 111 \rangle$ symmetry. The weak centre B was not studied in detail.

The small splitting of the EPR lines cannot be due to a misalignment of the crystal. However, it can be due to hf interaction with a nucleus with $I = \frac{1}{2}$ and ≈100% abundance. To examine this, ENDOR measurements were carried out. Figure 6 shows the ENDOR angular dependence measured on the three nonequivalent orientations of the trigonal centre when $\boldsymbol{B}$ is rotated in a $(01\bar{1})$ plane.

In the ENDOR experiment the information about the chemical identity of the nucleus (apart from the nuclear spin) is contained in the nuclear Zeeman interaction (the last term in (1)).

The EPR and ENDOR angular dependence (in the 16–35 MHz frequency range) can be described by the Hamiltonian (equation (1)) assuming that the paramagnetic centre interacts with a single ^{89}Y nucleus ($I = \frac{1}{2}$, $g_I = -0.274$). The values of the axially symmetric hf interaction tensor are given in table 3 in terms of the isotropic hf constant a and the anisotropic hf constant b, which are related to the principal values of the hf tensor by

$$A_{xx} = a - b \qquad A_{yy} = a - b \qquad A_{zz} = a + 2b. \tag{2}$$

The solid lines in figure 6 in the range between 16 and 36 MHz are ENDOR line positions

calculated using the parameters of the electron g-tensor and the ^{89}Y hf tensor listed in table 3.

The solid lines in figure 5 are EPR line positions calculated using the same parameters.

Additional ENDOR lines due to shf interactions with ^{133}Cs nuclei are found in the frequency region between 5 and 6.5 MHz. The angular dependence of these ENDOR lines (shown in the left-hand part of figure 6) has the same trigonal symmetry as the ^{89}Y angular dependence. Therefore, these lines must arise from shf interactions with those two of the eight nearest-neighbour ^{133}Cs nuclei that are situated on the trigonal ⟨111⟩ axis of the defect. The shf interaction parameters for this shell are given in table 3.

The Y^{2+} centres recombine with V_K centres in the temperature range between 60 and 84 K. In this annealing step the V_K-centre concentration is reduced by 50%. Further annealing to 170 K destroys the remaining V_K centres.

5. Discussion

5.1. The g-tensor and shf interaction parameters of the Y^{2+} centre

The magnitude of the ^{89}Y hf splitting suggests that yttrium is the central nucleus of this defect.

A paramagnetic charge state of yttrium that serves as an electron centre can only be a Y^{2+} defect that develops according to the following reaction:

$$Y^{3+} + e^- \rightarrow Y^{2+}. \tag{3}$$

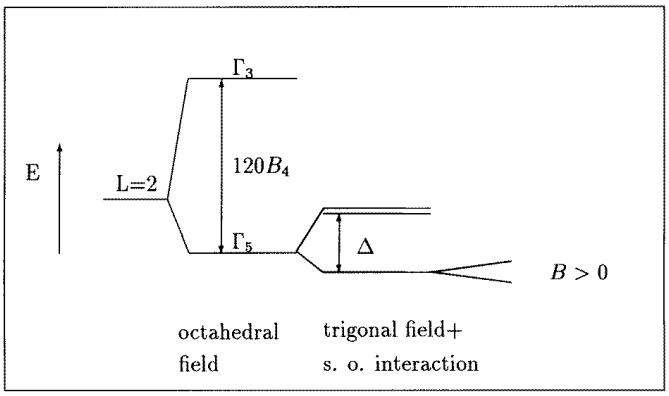

Figure 7. Energy levels of a $4d^1$ ion in an octahedral crystal field with trigonal distortion.

In the unperturbed lattice, Y^{3+} occupies a cubic site with an octahedron of Cl^- ions surrounding it. The ground state of Y^{2+} ($4d^1$) in this octahedral field is a Γ_5 orbital triplet. An additional crystal field with trigonal [111] symmetry removes the threefold degeneracy of the orbital triplet and yields a Kramers split ground state with trigonal symmetry of g- and hf tensors [14]. This energy level scheme is depicted in figure 7. The wavefunction of the ground state can be described as a $4d_{3z^2-r^2}$ function with the z-axis oriented along a trigonal ⟨111⟩ axis. This 4d wavefunction induces considerable spin density (via overlap) in the filled s shells of the Cs^+ ions along this ⟨111⟩ axis. Therefore it is understandable that the ^{133}Cs ENDOR lines arise from only those two of the eight nearest-neighbour Cs ions that are situated on the trigonal axis. A similar localization of spin density was found

in the case of the zinc vacancy in ZnSe [15] and the cadmium vacancy in CdTe [16]. These defects have a Jahn–Teller distorted Γ_5-type ground state.

The splitting Δ between the ground-state Kramers doublet and the two excited doublets (see figure 7) can be calculated from the deviation of $g_\parallel$ and $g_\perp$ from the free-electron value according to the following relations [14]:

$$g_\parallel = 2\cos^2\delta - 4\sin^2\delta \tag{4}$$

$$g_\perp = 2\cos^2\delta - 2\sqrt{2}\sin\delta\cos\delta \tag{5}$$

with

$$\tan 2\delta = \sqrt{2}\lambda/(\Delta + 1/2\lambda)$$

where λ is the spin–orbit interaction constant (300 cm^{-1} for Y^{2+}) [14].

Using the g-values determined in the EPR experiment, we calculate a splitting Δ of about 1500 cm^{-1}.

The hf interaction constants can be calculated as matrix elements of the operator equivalent $\boldsymbol{N}$ of the hf interaction and the eigenfunctions $\langle +|$ and $\langle -|$ of the Kramers split ground state according to [14]:

$$\begin{aligned} A_\parallel &= 2\langle +|N_z|+\rangle \\ A_\perp &= 2\,\mathrm{Re}\langle -|N_x|+\rangle. \end{aligned} \tag{6}$$

The result is

$$A_\parallel = \frac{2}{7}\langle r^{-3}\rangle_{4d}\left[2 - 8\sin^2\delta - 3\sqrt{2}\sin\delta\cos\delta\right] \tag{7}$$

$$A_\perp = \frac{2}{7}\langle r^{-3}\rangle_{4d}\left[1 + 2\sin^2\delta - 8\sqrt{2}\sin\delta\cos\delta\right] \tag{8}$$

with $\langle r^{-3}\rangle_{4d} = 2.323$ au^{-3} for Y^{2+} [14].

For $\Delta = 1500$ cm^{-1} we obtain $A_\parallel/h = -11.71$ MHz and $A_\perp/h = 21.07$ MHz.

An additional isotropic contribution to the shf tensor is the Fermi contact hf interaction a_c which is proportional to the unpaired spin density at the nuclear site. For the free Y^{2+} ion it was calculated using a program for solving the Dirac equation [17]. The result is $a_c = 77.57$ MHz.

The resulting values for the hf interaction constants are $A_\parallel/h = 65.86$ MHz and $A_\perp/h = 98.64$ MHz. The experimental observation that the absolute value of the parallel component of the shf tensor is smaller than the perpendicular component is confirmed by the calculation. Using the relations $a = \frac{1}{3}(A_\parallel + 2A_\perp)$ and $b = \frac{1}{3}(A_\parallel - A_\perp)$ we can finally calculate the isotropic and anisotropic shf interaction constants and obtain $a/h = 87.71$ MHz and $b/h = -10.92$ MHz.

Comparison of the calculated values of a and b with the experimental values from the ENDOR analysis (table 3) shows a very good agreement for the anisotropic part. The isotropic part deviates considerably. This value is strongly dependent on the value of the Fermi contact interaction, the calculation of which is not very precise [17].

There are two models that can explain the observed trigonal symmetry.

(i) The crystal contains Y^{3+} ions which are locally distorted by a defect in a $\langle 111\rangle$ direction.

(ii) The initial Y^{3+} ion is located on its natural unperturbed lattice site. When an electron is stabilized in a 4d orbital one would anticipate that the threefold degeneracy of the Γ_5 orbital triplet is removed by a local distortion of the complex (the Jahn–Teller effect). The distortion of the YCl_6 octahedron will have trigonal symmetry when the Γ_5 orbital multiplet

is coupled to a τ_2 vibrational mode [18]. A crude estimate of the splittings due to a static Jahn–Teller effect (following the calculations of Van Vleck [19] and Öpik and Pryce [20]) yields a value of approximately 900 cm^{-1}. The extra charge of Y^{2+} on the trivalent cation site should be compensated by a V_K centre in the neighbourhood.

Since the Jahn–Teller model accounts for both the symmetry and magnitude of the observed trigonal crystal field, the second model looks favourable. An interesting behaviour of the ENDOR spectra, which will be discussed later, supports this assignment.

At 4.9 K the width ΔB_{pp} of the Y^{2+} EPR lines is about 2.9 mT. Between 4.9 K and 12 K the linewidth is almost constant. Above 12 K the linewidth increases considerably to about 9.3 mT at 20 K. Above 20 K the EPR lines broaden beyond detection. This line broadening above 12 K can be attributed to a decrease in the spin–lattice relaxation time according to a second-order Raman process ($1/T_1 \propto T^9$), whereas below 12 K, the direct process ($1/T_1 \propto T$) is dominant.

5.2. Reorientation of the YCl_6 octahedron

The Y^{2+} ENDOR spectra display a very unusual behaviour. If one of the four centre orientations is selected for the ENDOR experiment via its anisotropic EPR spectrum, the ^{89}Y ENDOR spectrum shows lines due to other centre orientations whose corresponding EPR transitions are far away from the selected magnetic field value. The ENDOR signal from these other orientations is largest when the direction of the magnetic field is near to a ⟨111⟩ direction. For example, in a [111] direction where the EPR lines due to centre orientations 2, 3 and 4 coincide at 411 mT (see figure 5), the ENDOR spectrum measured at this magnetic field value also shows the two ($m_S = +1/2, m_S = -1/2$) lines from centre orientation 1 (at about 17 MHz). At this angle, however, the EPR transition corresponding to centre orientation 1 is at 360 mT (see figure 5) and should not be saturated in the ENDOR experiment.

To further illustrate this, figure 8 shows the ENDOR angular dependence measured only on the EPR line corresponding to the centre orientation marked 4 in figure 5. The ENDOR lines that belong to this orientation are shaded in figure 8. It can be seen that the ^{89}Y ENDOR spectrum also contains resonances from the other orientations (1, 2 and 3).

Two models have been considered to explain this observation.

(i) There are aggregates of two or more Y^{2+} centres with arbitrary orientations. The induction of an NMR transition at a centre which is not saturated and monitored by EPR can influence the saturation level of a nearby centre (which is monitored by EPR) via a cross-relaxation process.

(ii) The appearance of ENDOR lines from orientations that are not saturated by EPR is evidence for a reorientation of the YCl_6 octahedron.

Apart from a certain proximity of the centres, an effective cross-relaxation process also requires the conservation of energy, so there must be a partial overlap of the EPR spectra of the defects involved in cross relaxation. This is certainly not fulfilled in the case of the Y^{2+} centre, where for example for $\boldsymbol{B} \parallel [111]$ (where the effect is strongest) the EPR lines of centres 1 and 2–4 are separated by 50 mT (the EPR linewidth is only 2.9 mT). Thus the first possibility must be ruled out. The energy gap between the defects could in principle be bridged by phonons. However, this is unlikely at the low temperatures used in the experiment (≈5 K).

The second possibility looks much more favourable. One could imagine that if the nuclear relaxation time was long compared to the reorientation time of the centre, the

following process could occur: a NMR transition at the ^{89}Y nucleus changes the nuclear spin polarization when the defect is in centre orientation *a*. Due to the long relaxation time this change survives the reorientation to centre orientation *b*. The EPR only monitors centre orientation *b*, but due to the polarization memory the NMR transition in orientation *a* is also seen in the ENDOR spectrum measured in orientation *b*. The ENDOR linewidth could be used as an estimate of the lower limit of the reorientation time. From $\Delta f \approx 230$ kHz we get $T_{reor} > 4$ μs.

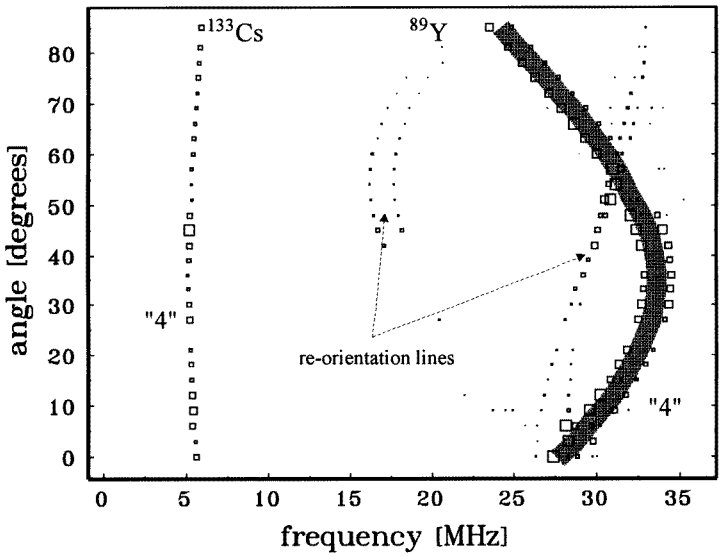

Figure 8. The ENDOR angular dependence of the trigonal Y^{2+} centre A measured on the EPR line marked 4 in figure 5.

All four centre orientations share the same ^{89}Y nucleus. However, the Cs neighbours that appear in the ^{133}Cs ENDOR spectrum are different in every orientation (because of the different trigonal centre axes). The spin memory process should, therefore, not work in the case of the ^{133}Cs ENDOR lines: if an NMR transition is induced at the Cs nuclei that are on the trigonal axis in orientation *a*, these nuclei are not on the axis when the centre reorients to orientation *b*. This absence of reorientational ENDOR lines in the ^{133}Cs ENDOR spectrum is indeed observed (compare the ^{133}Cs ENDOR lines in figure 8 with the ^{133}Cs ENDOR lines in the left-hand part of figure 6).

To our knowledge, a similar reorientational effect has been observed only in the ENDOR spectra of the $[Na]^0$ centre in CaO:Na^+ [21]. This paramagnetic defect is created in CaO:Na^+ as a hole centre by x-irradiation at 77 K. The hole is localized on one of the six equivalent oxygen neighbours that surround a Na^+ ion substituting for Ca^{2+}. The EPR spectrum is anisotropic with a prominent splitting due to shf interaction with the ^{23}Na nucleus.

It was proposed that even at 1.5 K the hole is partially delocalized and changes between the six oxygen neighbours. As in the case of the Y^{2+} centre, the evidence for this reorientation was the appearance of (^{23}Na) ENDOR lines from centre orientations that were not selected via EPR. In contrast to the case for the Y^{2+} centre, the reorientational lines come from shf interaction with a neighbouring nucleus. However, as in the case of Y^{2+}, this nucleus is a common neighbour of the hole centre in all six orientations.

6. Conclusion

We have studied two intrinsic x-irradiation-induced defects in Cs_2NaYCl_6. One of them is a V_K centre which is produced by x-irradiation at LN_2 temperatures, is thermally stable to about 150 K and has properties that are similar to those of the V_F centre in NaCl. At lower irradiation temperatures an intrinsic electron centre is produced which recombines with a proportion of the V_K centres at about 60–84 K. This centre was found to be a Jahn–Teller distorted Y^{2+} defect.

References

[1] O'Connor C J, Carlin R L and Schwartz R W 1977 *J. Chem. Soc. Faraday Trans.* **73** 361
[2] Bleaney B B, Stephen A G, Choh S H and Wells M R 1981 *Proc. R. Soc.* A **376** 253
[3] Schwartz R W and Hill N J 1974 *J. Chem. Soc. Faraday Trans.* **70** 124
[4] North M H and Stapleton H J 1977 *J. Chem. Phys.* **66** 4133
[5] Schwartz R W and Schatz P N 1973 *Phys. Rev.* B **8** 3229
[6] Van der Steen A C and Dirksen G J 1978 *Chem. Phys. Lett.* **59** 110
[7] Schwartz R W 1976 *Inorg. Chem.* **15** 2817
[8] Spaeth J-M, Hangleiter T, Koschnick F K and Pawlik Th 1995 *Radiat. Eff. Defects Solids* **135** 499
[9] Pawlik Th and Spaeth J-M 1996 *Proc. 13th ICDIM; Mater. Sci. Forum* **239–241** 287
[10] Itoh N 1972 *Cryst. Lattice Defects* **3** 115
[11] Castner G and Känzig W 1957 *J. Phys. Chem. Solids* **3** 178
[12] Spaeth J-M, Niklas J R and Bartram R H 1992 *Structural Analysis of Point Defects in Solids: An Introduction to Multiple Magnetic Resonance Spectroscopy (Springer Series in Solid State Sciences 43)* (Berlin: Springer)
[13] Känzig W 1960 *J. Phys. Chem. Solids* **17** 80
[14] Abragam A and Bleaney B 1970 *Electron Paramagnetic Resonance of Transition Ions* (New York: Dover)
[15] Jeon D, Gislason H P and Watkins G D 1993 *Phys. Rev.* B **48** 7872
[16] Emanuelsson P, Omling P, Wienecke M, Schenk M and Meyer B K 1993 *Phys. Rev.* B **47** 15 578
[17] Otte M 1992 *Diplomarbeit* University of Paderborn
[18] Bill H 1984 *The Dynamical Jahn–Teller Effect in Localized Systems* ed Yu E Perlin and M Wagner (Amsterdam: Elsevier)
[19] Van Vleck J H 1942 *J. Chem. Phys.* **7** 2015
[20] Öpik U and Pryce M H L 1957 *Proc. R. Soc.* A **238** 425
[21] Abraham M M, Unruh W P and Chen Y 1974 *Phys. Rev.* B **10** 3540